

# 1           **Long-term trends and drivers of aerosol pH in eastern China**

2   Min Zhou<sup>1,2</sup>, Guangjie Zheng<sup>3</sup>, Hongli Wang<sup>1</sup>, Liping Qiao<sup>1</sup>, Shuhui Zhu<sup>1</sup>, DanDan Huang<sup>1</sup>, Jingyu An<sup>1</sup>,  
3   Shengrong Lou<sup>1</sup>, Shikang Tao<sup>1</sup>, Qian Wang<sup>1</sup>, Rusha Yan<sup>1</sup>, Yingge Ma<sup>1</sup>, Changhong Chen<sup>1</sup>, Yafang Cheng<sup>3</sup>,  
4   Hang Su<sup>\*,1,4</sup>, Cheng Huang<sup>1</sup>

5  
6  
7   <sup>1</sup>State Environmental Protection Key Laboratory of the Cause and Prevention of Urban Air Pollution  
8   Complex, Shanghai Academy of Environmental Sciences, Shanghai200233, China

9   <sup>2</sup>School of Atmospheric Sciences, Nanjing University, Nanjing210023, China

10   <sup>3</sup>Minerva Research Group, Max Planck Institute for Chemistry, Mainz 55128, Germany

11   <sup>4</sup>Multiphase Chemistry Department, Max Planck Institute for Chemistry, Mainz 55128, Germany

12  
13   \*Corresponding author: Hang Su ([h.su@mpic.de](mailto:h.su@mpic.de))

## 20 Abstract

21 Aerosol acidity plays a key role in regulating the chemistry and toxicity of atmospheric aerosol particles.  
22 The trend of aerosol pH and its drivers are crucial in understanding the multiphase formation pathways  
23 of aerosols. Here, we reported the first trend analysis of aerosol pH from 2011 to 2019 in eastern China,  
24 calculated with ISORROPIA model based on observed gas and aerosol compositions. The  
25 implementation of the Air Pollution Prevention and Control Action Plan led to -35.8%, -37.6%, -9.6%, -  
26 81.0% and 1.2% changes of PM<sub>2.5</sub>, SO<sub>4</sub><sup>2-</sup>, NH<sub>x</sub>, non-volatile cations (NVCs) and NO<sub>3</sub><sup>-</sup> in the Yangtze  
27 River Delta (YRD) region during this period. Different from the fast changes of aerosol compositions  
28 due to the implementation of the Air Pollution Prevention and Control Action Plan, aerosol pH showed  
29 a minor/moderate change of -0.24 unit over the 9 years. Besides the multiphase buffer effect, the opposite  
30 effects from the changes of SO<sub>4</sub><sup>2-</sup> and non-volatile cations played key roles in determining the moderate  
31 pH trend, contributing to a change of +0.38 and -0.35 unit, respectively. Seasonal variations in aerosol  
32 pH were mainly driven by the temperature, while the diurnal variations were driven by both temperature  
33 and relative humidity. In the future, SO<sub>2</sub>, NO<sub>x</sub> and NH<sub>3</sub> emissions are expected to be further reduced by  
34 86.9%, 74.9% and 41.7% in 2050 according to the best health effect pollution control scenario (SSP1-  
35 26-BHE). The corresponding aerosol pH in eastern China is estimated to increase by ~0.19, resulting in  
36 4% more NO<sub>3</sub><sup>-</sup> and 12% more NH<sub>4</sub><sup>+</sup> partitioning/formation in the gas phase, which suggests that NH<sub>3</sub> and  
37 NO<sub>x</sub> emission controls are effective in mitigating haze pollution in eastern China.

38

## 39 1 Introduction

40 Aerosol acidity is an important parameter in atmospheric chemistry. It affects the particle mass and  
41 chemical composition by regulating the reactions of aerosols, and is closely associated with human health,  
42 ecosystems and climate (Li et al., 2017; Nenes et al., 2020b; Pye et al., 2020; Su et al., 2020). Aerosol  
43 acidity has attracted an increasing concern in recent years because of its impacts on the thermodynamics  
44 of gas-particle partitioning, pH-dependent condensed-phase reactions and trace metal solubility (Cheng  
45 et al., 2016; Fang et al., 2017; Guo et al., 2017b; Guo et al., 2016; He et al., 2018; Song et al., 2018;  
46 Weber et al., 2016; Su et al., 2020; Tilgner et al., 2021).

47 Thermodynamic models, such as E-AIM (Clegg et al., 1998) and ISORROPIA II are most commonly  
48 used for aerosol pH estimations, due to the limitations and difficulties in its direct measurements ~~of~~  
49 ~~aerosol pH~~ (Fountoukis and Nenes, 2007; Hennigan et al., 2015). ~~The Previously reported~~ aerosol pH  
50 ~~reported globally~~ generally ~~ranges-ranged~~ from -1 to 6 in the global scale (Pye et al., 2020; Zheng et al.,  
51 2020; Su et al., 2020). In United States, aerosols ~~are-were~~ reported to be highly acidic, with pH values of  
52 approximately 1–2 (Guo et al., 2015; Nah et al., 2018; Pye et al., 2018; Zheng et al., 2020). In comparison,  
53 aerosols in mainland China and Europe ~~are-were~~ generally less acidic with aerosol pH ranging between  
54 2.5 and 6 (Guo et al., 2018; Jia et al., 2018; Masiol et al., 2020; Shi et al., 2019; Tan et al., 2018; Wang  
55 et al., 2019; Zheng et al., 2020).

56 Aerosol pH exhibits notable spatial and temporal variability, which is affected by changes in factors  
57 such as temperature, relative humidity (RH), and aerosol compositions (Pye et al., 2018; Nenes et al.,  
58 2020a; Tao et al., 2020; Zheng et al., 2020). Very few studies have investigated the trend and spatial  
59 variability of aerosol pH and its drivers. Weber et al. (2016) showed that aerosols remained to be highly  
60 acidic even upon the reduction of particulate sulfate ( $\text{SO}_4^{2-}$ ) during summertime in the southeastern  
61 United States. Based on the 10-year observations conducted at six Canadian sites, Tao and Murphy (2019)  
62 suggested that meteorological parameters were more important than the chemical compositions in  
63 controlling aerosol pH. Zheng et al. (2020) found that aerosol liquid water content (ALWC) and  
64 temperature were the main factors that contribute to the pH difference observed between the wintertime  
65 North China Plain and summertime southeastern United States, whereas the change of chemical  
66 composition only played a minor role (15%). In China, the trend of aerosol pH and its drivers remain  
67 poorly understood, especially in recent years when the emissions and aerosol compositions changed  
68 substantially.

69 To tackle severe particulate matter pollution in China, the Chinese government released the Air  
70 Pollution Prevention and Control Action Plan (hereinafter referred to as the Action Plan) in September  
71 2013, which is the first plan specifying air quality goals in China (Cai et al., 2017; Liu et al., 2018; Zheng  
72 et al., 2018). The implementation of the Action Plan has led to significant changes in the concentrations  
73 and chemical compositions of fine particulate matter ( $\text{PM}_{2.5}$ ). Aerosol pH may change due to the  
74 significant changes of the chemical composition in  $\text{PM}_{2.5}$ , which may feedback to the multiphase  
75 formation pathways of aerosols such as sulfate, nitrate and ammonium (Cheng et al., 2016; Vasilakos et

76 al., 2018; Nenes et al., 2020a).

77 In this study, we performed a comprehensive analysis on the long-term trends of aerosol pH and its  
78 drivers in the Shanghai, China. A thermodynamic model, ISORROPIA II (version 2.1) (Fountoukis and  
79 Nenes, 2007) was applied to estimate the pH based on 9-year continuous online measurements of PM<sub>2.5</sub>  
80 composition at an urban site in Shanghai. The main purposes of this study are to: (1) characterize the  
81 long-term trend of aerosol pH; (2) investigate the seasonal and diurnal variations of aerosol pH and the  
82 main factors that affect these changes and (3) predict future pH under different emission control scenarios.  
83 The results presented here may help to advance our understanding in aerosol chemistry, providing a  
84 scientific basis on the development of effective pollution control strategy in the future.

## 85 2 Material and Methods

### 86 2.1 Ambient measurements

87 The observational site in this study is located at the Shanghai Academy of Environmental Sciences  
88 (SAES, 31°10'N, 121°25'E), which sits in the densely populated city centre of Shanghai (Figure S1). In  
89 the absence of significant nearby industrial sources, this sampling site represents a typical urban area of  
90 Shanghai affected by severe emissions from vehicular traffic, commercial, and residential activities (Qiao  
91 et al., 2014; Zhou et al., 2016).

92 Gases and PM<sub>2.5</sub> components were continuously sampled by an on-line analyser to monitor aerosols  
93 and gases (MARGA ADI 2080, Applikon Analytical B.V) from 2011 to 2019. Hourly mass  
94 concentrations of major inorganic components were obtained, including gaseous components, i.e., HCl,  
95 HNO<sub>2</sub>, SO<sub>2</sub>, HNO<sub>3</sub>, NH<sub>3</sub> and particulate components, i.e., SO<sub>4</sub><sup>2-</sup>, nitrate (NO<sub>3</sub><sup>-</sup>), chloride (Cl<sup>-</sup>),  
96 ammonium (NH<sub>4</sub><sup>+</sup>), sodium (Na<sup>+</sup>), potassium (K<sup>+</sup>), calcium (Ca<sup>2+</sup>) and magnesium (Mg<sup>2+</sup>). Details of  
97 measurements were have been given in Qiao et al. (2014), thus is are only briefly described here. To  
98 better track the changes in retention time of different ion species and ensure their concentrations were  
99 measured correctly, an internal standard check was conducted every hour with Lithium-lithium Bromide  
100 bromide (LiBr) standard solution (Qiao et al., 2014; Zhou et al., 2016). The sampling system of MARGA  
101 was cleaned and the multi-points calibrations with the standard solutions were performed every three  
102 months to ensure the accuracy of the measurements. To ensure the data quality, the ion balance between  
103 the measured charge equivalent concentrations of cation (NH<sub>4</sub><sup>+</sup>, Na<sup>+</sup>, K<sup>+</sup>, Ca<sup>2+</sup> and Mg<sup>2+</sup>) and anion

(SO<sub>4</sub><sup>2-</sup>, NO<sub>3</sub><sup>-</sup> and Cl<sup>-</sup>) species was examined as shown in Figure S2. Good correlation ( $R^2=0.94$ ) was found between the cations and anions, suggesting very good data quality during the measurement period. We note that data during 2011-2016 were more scattered than those during 2017-2019, likely due to the significant decreases in Ca<sup>2+</sup>, K<sup>+</sup> and Mg<sup>2+</sup> from 2011 to 2019 (Figure S3-S5). In previous studies, intercomparison experiments between MARGA and filter-based method have been carried out, and the data measured by MARGA showed acceptable accuracy and precision (Rumsey et al., 2014; Huang et al., 2014; Stieger et al., 2018). A Thermal/Optical Carbon Aerosol Analyzer (model RT-4, Sunset laboratory Inc.) equipped with a PM<sub>2.5</sub> cyclone was used for the organic carbon measurement at a time resolution of 1 hour. The mass concentrations of PM<sub>2.5</sub> were simultaneously measured using an on-line beta attenuation PM monitor (FH 62 C14 series, Thermo Fisher Scientific) at a time resolution of 5 min.

Temperature and RH, which are important factors affecting aerosol pH, were also measured at a time resolution of 1 min. Annually averaged temperature and RH from 2011 to 2019 are shown in Figure S6. The t-test results revealed that temperature rose significantly at a rate of 1.2 %/yr ( $p < 0.01$ ), while RH changed little.

## 2.2 Aerosol pH prediction

The aerosol pH was predicted using the ISORROPIA II thermodynamic model (Fountoukis and Nenes, 2007). ISORROPIA II can calculate the equilibrium  $H_{air}^+$  and aerosol liquid water content of inorganic material ( $ALWC_i$ ) by inputting the concentrations of the total SO<sub>4</sub><sup>2-</sup> (TH<sub>2</sub>SO<sub>4</sub>, replaced by observed SO<sub>4</sub><sup>2-</sup>), total NO<sub>3</sub><sup>-</sup> (TNO<sub>3</sub>, gas HNO<sub>3</sub> plus particle NO<sub>3</sub><sup>-</sup>), total ammonia (NH<sub>x</sub>, gas NH<sub>3</sub> plus particle NH<sub>4</sub><sup>+</sup>), total Cl<sup>-</sup> (TCl, replaced by observed Cl<sup>-</sup> due to the low concentration and measurement uncertainties of HCl) (Fu et al., 2015; Ding et al., 2019), non-volatile cations (NVCs, observed Na<sup>+</sup>, K<sup>+</sup>, Ca<sup>2+</sup>, Mg<sup>2+</sup>) and meteorological parameters (temperature and RH) (Guo et al., 2016).  $H_{air}^+$  and  $ALWC_i$  are then used to obtain the PM<sub>2.5</sub> pH by Eq. (1).

$$pH = -\log_{10} H_{aq}^+ \cong -\log_{10} \frac{1000H_{air}^+}{ALWC_i + ALWC_o} \cong -\log_{10} \frac{1000H_{air}^+}{ALWC_i}, \quad (1)$$

where  $H_{aq}^+$  is the H<sup>+</sup> concentration in solution (mol/L),  $H_{air}^+$  is the H<sup>+</sup> loading for an air sample (μg/m<sup>3</sup>) and  $ALWC_i$  and  $ALWC_o$  are the aerosol liquid water contents of inorganic and organic species, respectively (μg/m<sup>3</sup>).  $ALWC_o$  is calculated by Eq. (2) (Guo et al., 2015).

$$ALWC_o = \frac{m_{org}\rho_w}{\rho_{org}} \frac{k_{org}}{\left(\frac{1}{RH}-1\right)}, \quad (2)$$

where  $m_{org}$  is the mass concentration of organic aerosol,  $\rho_w$  is the density of water ( $\rho_w=1.0\text{g/cm}^3$ ),  $\rho_{org}$  is the density of organics ( $\rho_{org}=1.4\text{g/cm}^3$ ) (Guo et al., 2015), and  $k_{org}$  is the hygroscopicity parameter of organic aerosol ( $k_{org} = 0.087$ ) (Li et al., 2016). The concentration of organic aerosol was estimated by multiplying the measured concentration of organic carbon by a factor of 1.6 (Turpin and Lim, 2001). The average concentrations of  $ALWC_o$  and  $ALWC_i$  in Shanghai from 2011 to 2019 were  $4.1 (\pm 10.2)$  and  $32.6 (\pm 52.5) \mu\text{g/m}^3$ , respectively.  $ALWC_o$  only accounted for 11.1% of the total aerosol liquid water content. The pH predictions in previous studies were insensitive to  $ALWC_o$  unless the mass fraction of  $ALWC_o$  to the total aerosol liquid water content was close to unity (Guo et al., 2015). The use of  $ALWC_i$  to predict pH is therefore fairly accurate and common (Battaglia et al., 2017; Ding et al., 2019; Battaglia Jr et al., 2019). In this study, ISORROPIA II was run in the forward mode and ‘metastable’ state. Calculations using total (gas and aerosol) measurements in the forward mode are less affected by measurement errors (Hennigan et al., 2015; Song et al., 2018). A detailed description of the pH calculations can be found in previous studies (Guo et al., 2017a; Guo et al., 2015; Song et al., 2018).

Figure S6-S7 compares the predicted vs. measured concentrations of  $\text{NH}_3$ ,  $\text{NH}_4^+$ ,  $\text{NO}_3^-$  and  $\text{HNO}_3$ . The results show that the predicted and measured concentrations of  $\text{NH}_3$ ,  $\text{NH}_4^+$  and  $\text{NO}_3^-$  are in good agreement ( $R^2 > 0.89$ ) and slopes close to 1.00, indicating that the thermodynamic analysis accurately represents the aerosol state and that deviations in the calculated pH values are lower than that in modelled  $\text{NH}_3$  (Weber et al., 2016). However, the predicted and measured concentrations of  $\text{HNO}_3$  are not well ~~corrected~~ correlated, which is also observed in previous studies (Ding et al., 2019; Guo et al., 2015). The reason for the gap can be attributed to (1) lower concentrations of gas-phase  $\text{HNO}_3$  than that of particle-phase  $\text{NO}_3^-$ , (2)  ~~$\text{HNO}_3$  measurement by MARGA~~ are has high uncertainty for  $\text{HNO}_3$  measurement (Rumsey et al., 2014). The development of an alternative approach is therefore warranted to accurately represent  $\text{HNO}_3$  in the future.

### 2.3 Drivers of aerosol pH variations

To investigate the factors that drive changes in aerosol pH, sensitivity tests of different factors on pH variations, including temperature, RH,  $\text{SO}_4^{2-}$ ,  $\text{TNO}_3$ ,  $\text{NH}_x$ ,  $\text{Cl}^-$  and NVCs, were performed with the one-

160 at-a-time method. That is, assuming the aerosol pH estimated under scenario I ( $pH_I$ ) differs ~~with-from~~  
161 that under scenario II ( $pH_{II}$ ), the pH difference, ( $\Delta pH = pH_{II} - pH_I$ ), are thus caused by the variations in  
162 the factors listed above. To quantify the contributions of individual factors, we varied the factor  $i$  from  
163 the value in scenario I to another value in scenario II and meanwhile kept the other factors fixed. The  
164 corresponding changes in pH,  $\Delta pH_i$ , are assumed to represent the contribution of the change of this  
165 individual factor to the overall aerosol pH variations. The unresolved contributors to pH differences, i.e.,  
166  $\Delta pH - \sum_i \Delta pH_i$ , are attributed to “others”, which may represent the contribution of covariations between  
167 the factors. Note that because of the nonlinear dependence of pH to different factors, the sum of  
168 contributions of individual factors can be slightly different from the overall contributions of all factors.  
169 This method was used for the results presented in Figure 1b, Figure 3 and Figure 5, where the  
170 corresponding scenarios represented the average conditions in different years (Figure 1b), seasons  
171 (Figure 3) or diurnal periods (Figure 5).

## 172 3 Results and Discussion

### 173 3.1 Long-term trends of aerosol pH

#### 174 3.1.1 Trends of aerosol pH.

175 The 9-year time series of aerosol pH calculated by ISORROPIA II is shown in Figure 1a. A declining  
176 trend in  $PM_{2.5}$  pH from  $3.30 \pm 0.58$  in 2011 to  $3.06 \pm 0.55$  in 2019 was observed, with the fitted decrease  
177 rate of around 0.04 ~~unit-pH~~ per year, which may be related to chemical composition changes (Figure  
178 ~~S78-S8S9~~) due to the pollution control measures taken in the Yangtze River Delta (YRD) region. The  
179 Chinese government started to ~~implement-carry on~~ the Action Plan, a series of air pollution control  
180 policies, in September 2013, which resulted in a decline in  $PM_{2.5}$  and its chemical components (Cheng et  
181 al., 2019; Li et al., 2019). Compared to the concentrations before the ~~implement~~ ation of the Action Plan  
182 (i.e., average of 2011-2012 averages),  $PM_{2.5}$ ,  $SO_4^{2-}$ ,  $NH_x$  and NVCs during 2018-2019 decreased by  
183 35.8%, 37.6%, 9.6% and 81.0%, respectively, while  $NO_3^-$  increased by 1.2% (Fig. ~~S7S8~~). Through the  
184 years,  $SO_4^{2-}$ ,  $NH_4^+$  and  $NO_3^-$  ~~were kept being remained~~ the most abundant inorganic water-soluble ions,  
185 accounting for 83.4%–94.1% of the total ions in  $PM_{2.5}$ . While the proportions of  $NH_4^+$  and  $NO_3^-$  showed  
186 continuous increases (~~increased~~ by 2.2% and 13.1% from 2011 to 2019, ~~respectively~~), those of NVCs

187 and  $\text{SO}_4^{2-}$  decreased by 6.0% and 4.6%, respectively. Despite the substantial change of aerosol abundance  
188 and composition, the aerosol pH only ~~showed~~ shows a ~~moderate~~ minor change. The effects of changes  
189 in  $\text{PM}_{2.5}$  chemical composition on the aerosol pH will be detailed in Section 3.1.2.

190 The  $\text{PM}_{2.5}$  in Shanghai was moderately acidic with a daily pH ~~averaging 3.18 and ranging range~~ from  
191 1.15 to 5.62, similar to those from other cities in China (Shi et al., 2019; Tan et al., 2018). Compared  
192 with other countries globally (Table S1), aerosol pH ~~values~~ in Chinese cities ~~of 1.82 to 5.70~~ were higher  
193 than those in US cities ~~of 0.55 to 2.20~~ (Guo et al., 2015; Pye et al., 2018; Nah et al., 2018), yet similar to  
194 those in European cities ~~of 2.30 to 3.90~~ (Guo et al., 2018; Masiol et al., 2020). Among all of the Chinese  
195 cities, the aerosol pH was highest in Inner Mongolia, which might be caused by a higher contribution of  
196 crustal dust ~~in Inner Mongolia~~ (Wang et al., 2019). The pH values in Shanghai and Guangzhou were  
197 lower than those in North China, which may be due to higher concentrations of  $\text{NH}_3$  and dust emissions  
198 over the latter region (Shi et al., 2007; Liu et al., 2019).

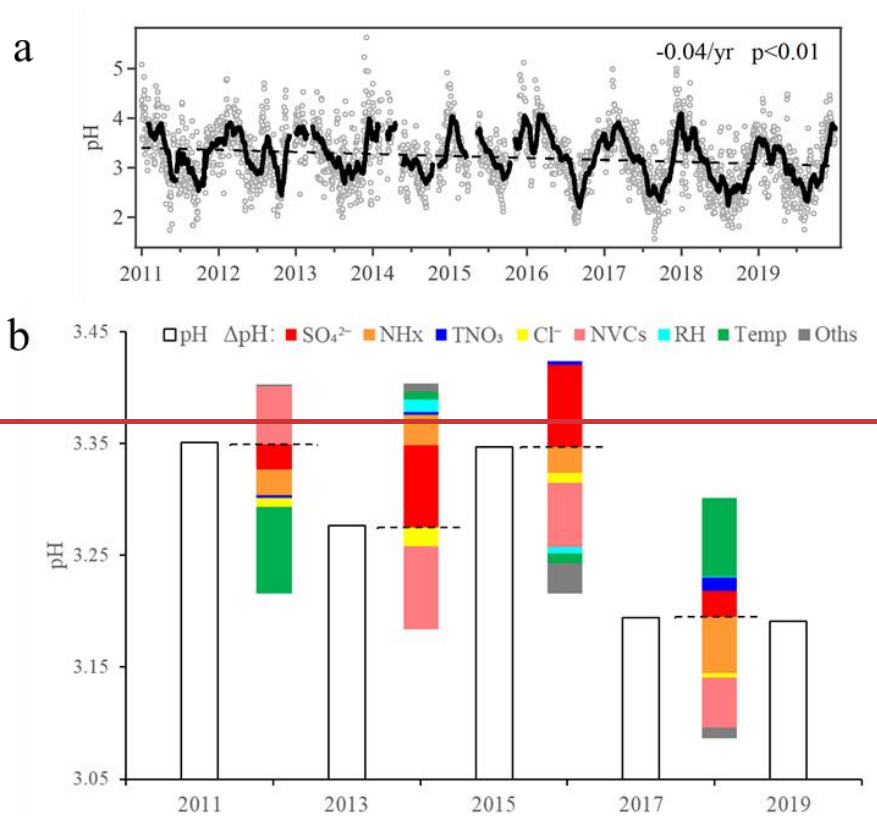
### 199 3.1.2 Driving factors.

200 Figure 1b shows the contributions of individual factors to the  $\Delta\text{pH}$  from 2011 to 2019. Here the bar plots  
201 indicate the factors contributing to the  $\Delta\text{pH}$  between two adjacent scenarios as shown in Figure 1b, e.g.,  
202 2011 to 2013. See Figure ~~S9a-S10a~~ for the factor contribution to the variation from average conditions.  
203 Note that in Fig. 1b, the aerosol pH was calculated from the annual averages of input parameters. This is  
204 different from Sect 3.1.1, where the annual pH is the average of hourly values based on hourly  
205 observation data. As shown in Figure 1b, the aerosol pH decreased from 3.35 in 2011 to 3.28 in 2013.  
206 The main factors that affected the pH during 2011-2013 (prior to the implementation of the Action Plan)  
207 were the temperature and NVCs. The pH value also continuously decreased from 3.28 in 2013 to 3.19 in  
208 2019. Yet,  $\Delta$  chemical composition shows more prominent effects on the aerosol pH during 2013-2019  
209 compared to that of 2011-2013. As aforementioned, upon implementation of the Action Plan (2013-2019),  
210 the concentrations of  $\text{PM}_{2.5}$  and its chemical components decreased substantially (Figure ~~S7S8~~). Changes  
211 of  $\text{SO}_4^{2-}$  and NVCs were important determinants in the change of aerosol pH, resulting in  $\Delta\text{pH}$  of +0.38  
212 ~~units~~ and ~~-0.35 units~~ ~~respectively~~ from 2013 to 2019, ~~respectively~~. Changes in the  $\text{NH}_x$  and  $\text{Cl}^-$  were  
213 associated with 0.08 and 0.06 decreases in  $\Delta\text{pH}$ , respectively, whereas  $\text{TNO}_3$  had little impact on the  $\Delta\text{pH}$ .  
214 Hence, besides the effect of reduction in  $\text{SO}_4^{2-}$  (Fu et al., 2015; Xie et al., 2020), our results suggest that  
215 the change in NVCs may also play an important role in determining the trend of aerosol pH. During



216 2017-2019, we found temperature and  $\text{NH}_x$  became the main drivers of the  $\Delta\text{pH}$ . The effects of  $\text{SO}_4^{2-}$   
217 and NVCs on pH were much weaker than those during 2013–2017, consistent with the fact that the  
218 decline in pollutant concentrations slowed down in recent years (Fig. S8S9).

219 Overall, the changes in  $\text{SO}_4^{2-}$  and NVCs were the main drivers of the  $\Delta\text{pH}$  upon the implementation  
220 of the Action Plan, and  $\text{NH}_x$  appeared to play an increasingly important role in determining the aerosol  
221 pH through the years.



222

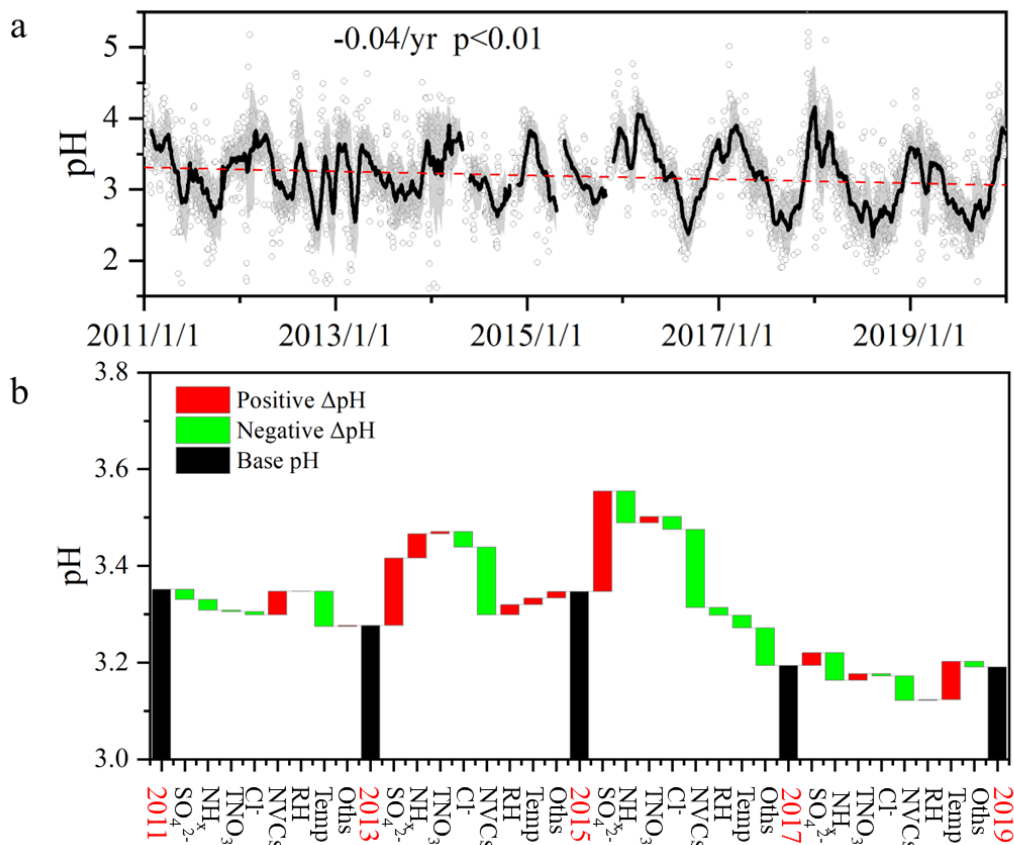


Figure 1. (a) Long-term trends in aerosol pH during 2011–2019 in Shanghai. Gray dots and black lines represent the daily pH values and 30-day moving average pH values, respectively. Shaded areas mark the standard deviation of 30-day moving average pH values. (b) Contributions of individual factors to the  $\Delta\text{pH}$  from 2011 to 2019. Here the black bars plots indicate the mean pH of different years, and the red and green bars represent the factors positive and negative effects of individual factors on  $\Delta\text{pH}$  between two adjacent scenarios, e.g., 2011 to 2013, respectively. contributing to the  $\Delta\text{pH}$  between two adjacent scenarios, e.g., 2011 to 2013. The stacked color bars below the dashed line represent the factors that had negative impacts on  $\Delta\text{pH}$ , and the stacked color bars above the dashed line represent the factors that had positive impacts on  $\Delta\text{pH}$ . The meanings of the abbreviations: RH, relative humidity; Temp, temperature; NVCs, non-volatile cations;  $\text{NH}_x$ , total ammonia;  $\text{TNO}_3$ , total nitrate; Oths, others.

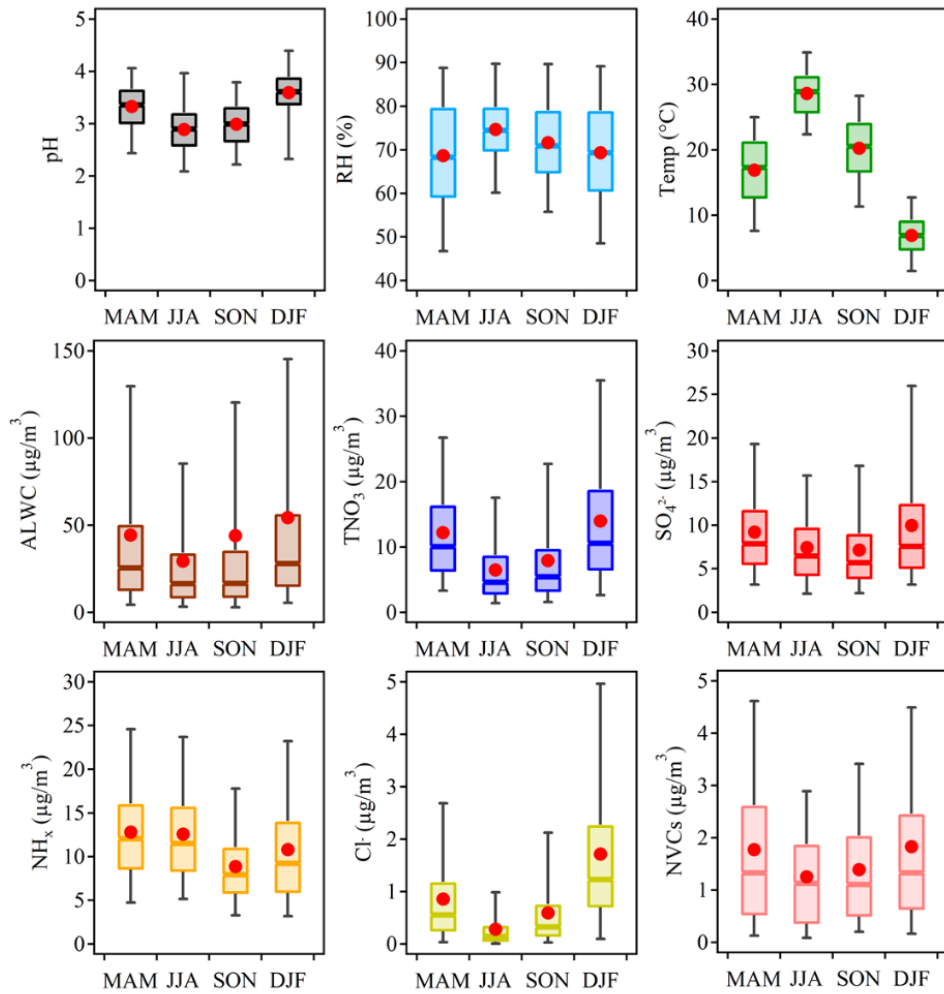
### 3.2 Seasonal variation

Figure 2 shows the seasonal variations of aerosol pH in Shanghai. The average pH values were  $3.33 \pm 0.49$ ,  $2.89 \pm 0.49$ ,  $2.99 \pm 0.52$  and  $3.59 \pm 0.57$  in spring (March–May, MAM), summer (June–August, JJA), fall (September–November, SON) and winter (December–February, DJF), respectively. The

238 highest aerosol pH was found in winter while the lowest pH was found in summer. While ~~similar-the~~  
239 seasonal variations of pH in Shanghai were similar to those observed in Beijing and other NCP cities  
240 (Tan et al., 2018; Ding et al., 2019; Shi et al., 2019; Wang et al., 2020), the absolute values were lower,  
241 due to the generally lower concentrations of aerosol chemical compositions in YRD.

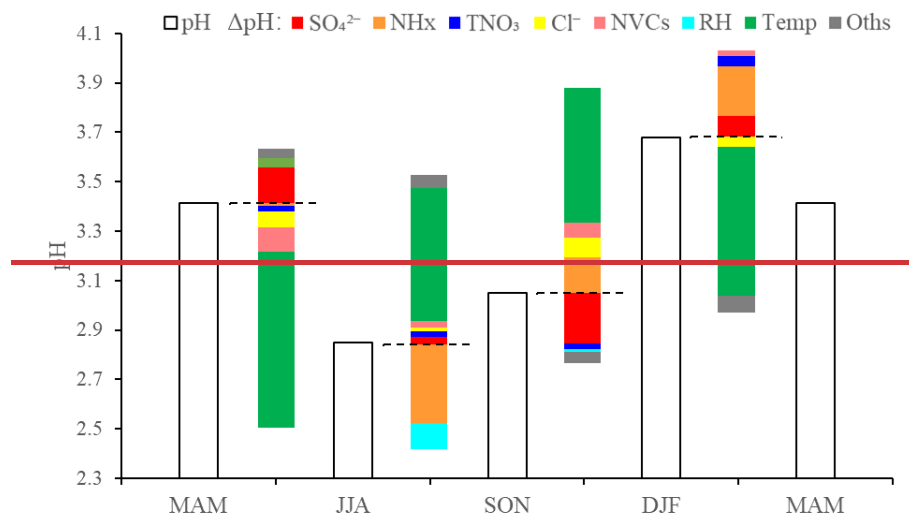
242 Figure 3 shows the contributions of individual factors to the  $\Delta\text{pH}$  across the four seasons. Here the bar  
243 plots indicate the factors contributing to the  $\Delta\text{pH}$  between two adjacent seasons, e.g., spring (MAM) to  
244 summer (JJA). See ~~Figure S9b-S10b~~ for the factor contribution to the variation from average conditions.  
245 The aerosol pH was calculated from the mean averages of input parameters in four seasons, and the  $\Delta\text{pH}$   
246 was estimated by varying one factor while holding the other factors fixed in different seasons. According  
247 to the multiphase buffer theory, the peak buffer pH,  $\text{p}K_{\text{a}}^*$  regulates the aerosol pH in a multiphase-  
248 buffered system, and temperature can largely drive the seasonal variation of aerosol pH through its impact  
249 on  $\text{p}K_{\text{a}}^*$  (Zheng et al., 2020). This is evidenced by the results in Figure 3, as temperature shows a dominant  
250 role in driving the seasonal variation of aerosol pH. The temperature was associated with a maximum  
251  $\Delta\text{pH}$  of 0.63 from fall to winter. Besides temperature, ~~the other two~~ main factors ~~affecting aerosol pH~~  
252 were  $\text{NH}_x$  and  $\text{SO}_4^{2-}$  (Figure 3), contributing 16% and 12% of the changes, respectively. Our results  
253 suggest a central role of temperature in the determination of seasonal variations in aerosol pH, consistent  
254 with the results of Tao and Murphy (Tao and Murphy, 2019) at six Canadian sites and the prediction by  
255 the multiphase buffer theory (Zheng et al., 2020). In comparison, some previous studies emphasized the  
256 importance of chemical compositions in seasonal variations (Tan et al., 2018; Ding et al., 2019), which  
257 is mainly due to the different sensitivity analysis methods applied.

258

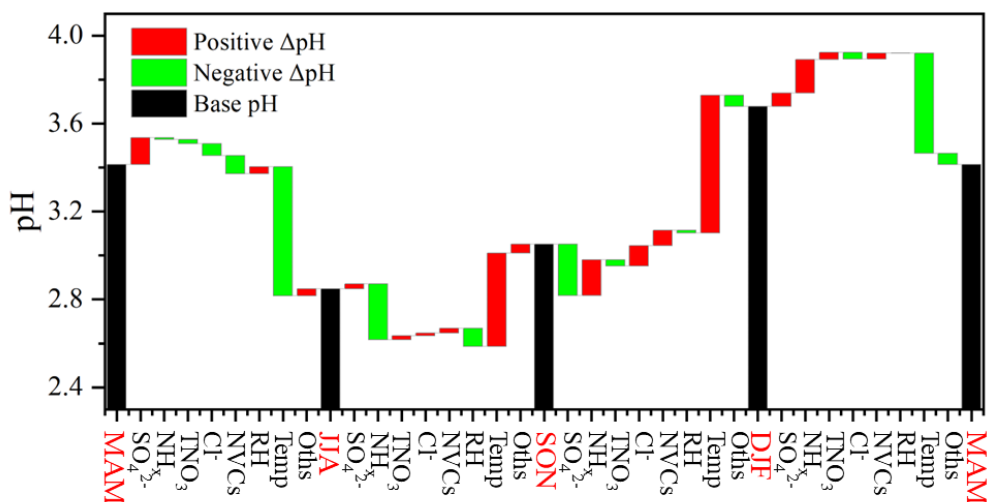


259

260 **Figure 2. Seasonal variations of the mass concentrations of major components in PM<sub>2.5</sub>, relative humidity**  
 261 **(RH), temperature (Temp), predicted aerosol liquid water content (ALWC) and aerosol pH during 2011–2019**  
 262 **in Shanghai.**



263



264

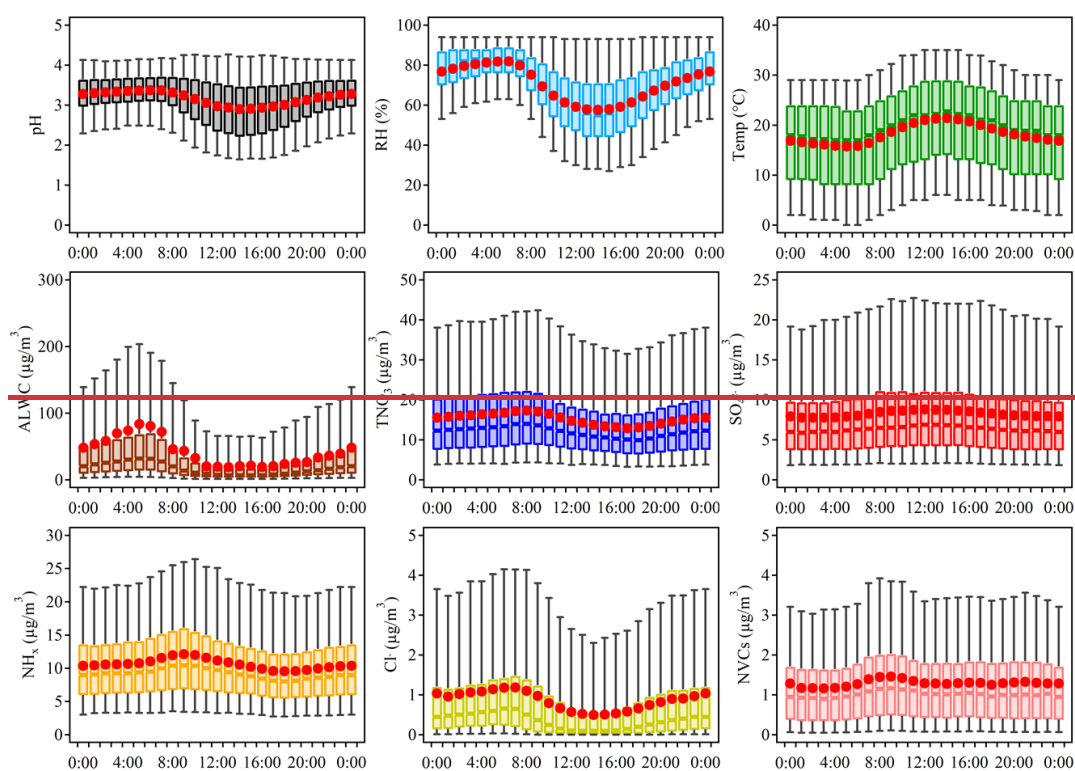
265 **Figure 3. Contributions of individual factors to the  $\Delta$ pH across the four seasons. Here the black bars plots**  
 266 **indicate the factors contributing to the  $\Delta$ pH between two adjacent seasons, e.g., spring (MAM) to summer**  
 267 **(JJA). The stacked color bars below the dashed line represent the positive and negative effects of individual factors on  $\Delta$ pH between two adjacent scenarios, e.g.,**  
 268 **spring (MAM) to summer (JJA), respectively.**the factors contributing to the  $\Delta$ pH between two adjacent  
 269 **seasons, e.g., spring (MAM) to summer (JJA). The stacked color bars below the dashed line represent the**  
 270 **factors that had negative impacts on  $\Delta$ pH and the stacked color bars above the dashed line represent the**  
 271 **increase in  $\Delta$ pH.** The meanings of the abbreviations: RH, relative humidity; Temp, temperature; NVCs, non-  
 272 **volatile cations; NH<sub>x</sub>, total ammonia; TNO<sub>3</sub>, total nitrate; Oths, others.**  
 273

### 274 3.3 Diurnal variation

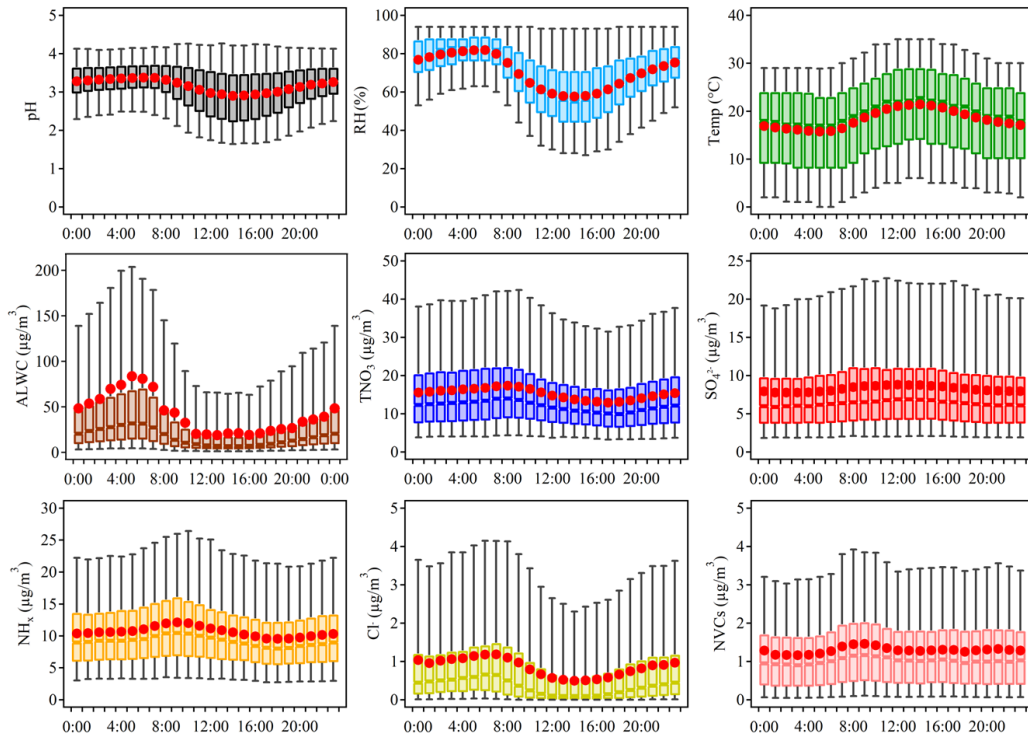
275 Aerosol pH in Shanghai exhibits notable diurnal variations with high aerosol acidity observed during  
 276 daytime. Diurnal variations of aerosol pH as well as those of its potential drivers were arc depicted in  
 277 Figure 4. We further explore the effects of individual factors on the  $\Delta$ pH between day and night through  
 278 sensitivity tests.

279 The Bbar plot in Figure 5 indicates the factors contributing to the  $\Delta$ pH between two adjacent hour  
 280 periods, e.g., 0:00 to 6:00. See Figure S9e-S10c for the combined effects of contributions from different  
 281 factors on the average  $\Delta$ pH. The aerosol pH was calculated from the averages of input parameters in 0:00,  
 282 6:00, 12:00 and 18:00, and  $\Delta$ pH was estimated by varying one factor while holding the other factors  
 283 fixed in different hours. Temperature and RH were among the main drivers of the diurnal variation of

284 aerosol pH, with a maximum  $\Delta$ pH of -0.22 and +0.10 units, respectively. As shown in Figure 4, the  
 285 maximum RH and ALWC occurred at approximately 5:00. After sunrise, the increase in temperature  
 286 resulted in an immediate drop of RH with ALWC reached-reaching its lowest level in the afternoon.  
 287 Accordingly, the minimum aerosol pH ( $\sim$ 2.8) was also found in the afternoon with high temperature and  
 288 low RH. After sunset, the decreasing temperature and increasing RH led to a highest aerosol pH overnight.  
 289 Minor changes in pH were found between 0:00 and 6:00, when temperature and RH also showed minor  
 290 changes. The impacts of other factors, such as  $\text{SO}_4^{2-}$ , on the diurnal variations of pH were notably smaller  
 291 than on seasonal variations, which may be attributed to the relatively small variations of chemical profiles  
 292 during the course of a day. Among the chemical compositions,  $\text{NH}_x$  played the most important role,  
 293 followed by  $\text{SO}_4^{2-}$ . Overall, temperature and RH were more important than chemical compositions in  
 294 regulating the diurnal variations of aerosol pH.



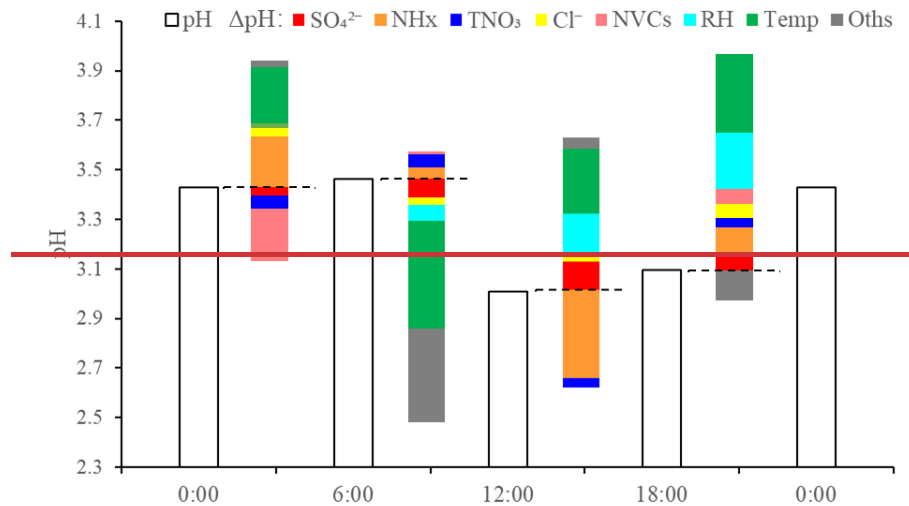
295



296

297 **Figure 4. Diurnal variations of the mass concentrations of major ions in PM<sub>2.5</sub>, relative humidity (RH),**  
 298 **temperature (Temp), predicted aerosol liquid water content (ALWC) and aerosol pH during 2011–2019 in**  
 299 **Shanghai.**

300



301

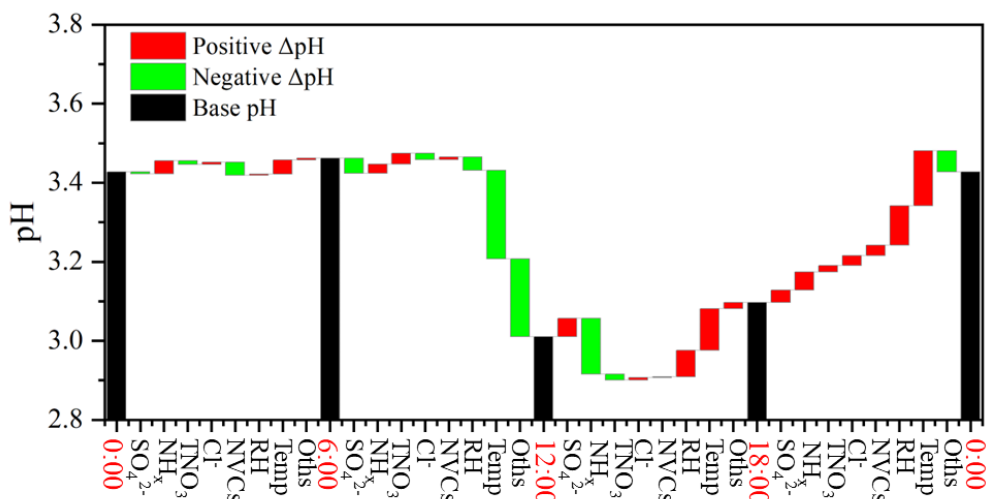


Figure 5. Contributions of individual factors to the  $\Delta\text{pH}$  between day and night. Here the **black bars plots** indicate **the mean pH of different hours, and the red and green bars represent the positive and negative effects of individual factors on  $\Delta\text{pH}$  between two adjacent scenarios, e.g., 0:00 to 6:00, respectively, the factors contributing to the  $\Delta\text{pH}$  between two adjacent hour periods, e.g., 0:00 to 6:00. The stacked color bars below the dashed line represent the factors that had negative impacts on  $\Delta\text{pH}$  and the stacked color bars above the dashed line represent the increase in  $\Delta\text{pH}$ .** The meanings of the abbreviations: RH, relative humidity; Temp, temperature; NVCs, non-volatile cations;  $\text{NH}_x$ , total ammonia;  $\text{TNO}_3$ , total nitrate; Oths, others.

### 3.4 Future projections

A series of prevention and control measures have been suggested for continuous improvement in air quality, which will affect the particulate compositions and subsequently alter the aerosol pH in China. To explore China's future anthropogenic emission pathways in 2015–2050, [Tong et al.](#) (2020) developed a dynamic projection model, based on which different emission scenarios were created by connecting five socio-economic pathway (SSP) scenarios, five representative concentration pathways (RCP) scenarios (RCP8.5, 7.0, 6.0, 4.5 and 2.6) and three pollution control scenarios (business as usual, BAU; enhanced control policy, ECP; and best health effect, BHE). These scenarios provide a better understanding of the future trends in pollutant emissions. (Tong et al., 2020).

In this study, we chose three different emission reduction scenarios (SSP3-70-BAU, SSP2-45-ECP, and SSP1-26-BHE) as the future anthropogenic emission pathways, and based on which we try to project the future aerosol pH levels in Shanghai. SSP1-26-BHE, which involves a combination of strong low-



322 carbon and air pollution control policy, has the greatest emission reduction, followed by SSP2-45-ECP.  
323 SSP3-70-BAU is a reference scenario ~~that~~ without additional efforts to constrain emissions. We first  
324 tested the sensitivity of aerosol abundances to precursor emissions with the historical data (Figure  
325 ~~S10~~S11), the emissions of Shanghai were obtained by the Multi-resolution Emission Inventory for China  
326 (MEIC, <http://meicmodel.org/>, last access: 15 January 2020). We found that the non-volatile sulfate  
327 concentrations generally correlated linearly with that of the SO<sub>2</sub> emissions. For the volatile TNO<sub>3</sub> and  
328 NH<sub>x</sub>, the correlations are less linear, likely due to the different deposition velocities of gases and particles  
329 (Pye et al., 2020; Weber et al., 2016; Nenes et al., 2021). The historical emission reductions have resulted  
330 in a moderate pH decrease (Figure 1), a moderate increase (0.2% per year) in the NO<sub>3</sub><sup>-</sup> partitioning, and  
331 a decrease (-0.6% per year) in the NH<sub>4</sub><sup>+</sup> partitioning (Figure ~~S11~~S12).

332 For a first-order estimation, we applied the average  $\Delta$ aerosol/ $\Delta$ precursor emissions in ( $\mu\text{g}/\text{m}^3$ )/  
333 (Gg/yr) as derived from the historical (Figure ~~S10a~~S11a-c) to the future scenario predictions. Figure 6  
334 shows the emissions of SO<sub>2</sub>, NO<sub>x</sub>, NH<sub>3</sub> and predicted pH levels and the effects of major chemical  
335 components (NH<sub>x</sub>, SO<sub>4</sub><sup>2-</sup>, and TNO<sub>3</sub>) to the  $\Delta$ pH in Shanghai from 2015 to 2050 under the three scenarios.  
336 Based on this assumption, the concentrations of SO<sub>4</sub><sup>2-</sup>, NO<sub>3</sub><sup>-</sup> and NH<sub>4</sub><sup>+</sup> are expected to drop to ~6.3, 5.7  
337 and 2.6  $\mu\text{g}/\text{m}^3$ , respectively in 2050 with the SSP1-26-BHE scenario, generally in agreement with the  
338 predicted PM<sub>2.5</sub> levels of ~15  $\mu\text{g}/\text{m}^3$  under such scenario (Shi et al., 2021).

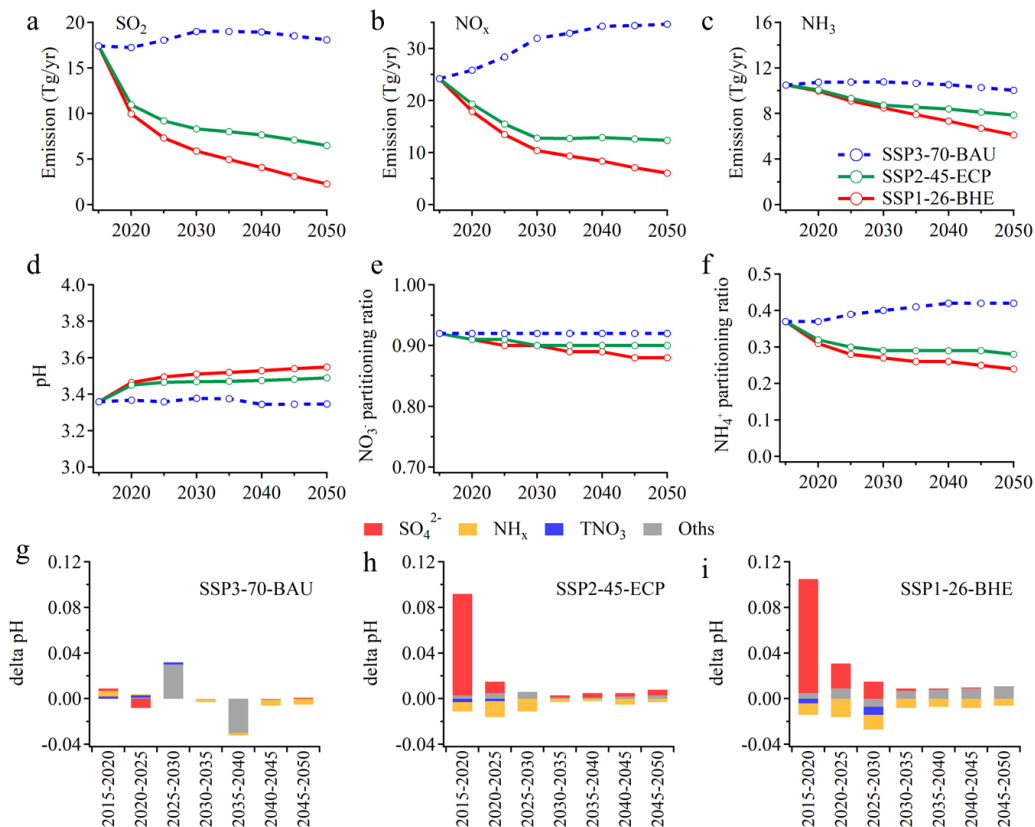
339 Under the reference scenario of SSP3-70-BAU with weak control policy (blue dashed lines in Figure  
340 6a-f), SO<sub>2</sub> and NO<sub>x</sub> are predicted to increase, while ~~the~~ NH<sub>x</sub> is relatively stable. NH<sub>x</sub>, SO<sub>4</sub><sup>2-</sup>, and TNO<sub>3</sub>  
341 have minor effects on  $\Delta$ pH (Figure 6g). Correspondingly, there are little changes in aerosol pH and the  
342 predicted NO<sub>3</sub><sup>-</sup> partitioning ratio (NO<sub>3</sub><sup>-</sup> / (NO<sub>3</sub><sup>-</sup> + HNO<sub>3</sub>)). However, the NH<sub>4</sub><sup>+</sup> partitioning ratio (NH<sub>4</sub><sup>+</sup> /  
343 (NH<sub>4</sub><sup>+</sup> + NH<sub>3</sub>)) will increase substantially, suggesting an enhanced formation of ammonium aerosols.

344 Under the moderate control policy (SSP2-45-ECP), the emissions of SO<sub>2</sub>, NO<sub>x</sub>, and NH<sub>3</sub> in 2050 will  
345 be reduced by 62.7%, 49.0% and 25.0%, respectively with corresponding decreases in SO<sub>4</sub><sup>2-</sup>, TNO<sub>3</sub> and  
346 NH<sub>x</sub>. The predicted pH will increase by ~0.13, and the NH<sub>4</sub><sup>+</sup> partitioning ratio will decrease by 0.09,  
347 indicating that relatively more ammonium will exist in the gas phase as NH<sub>3</sub>. The NO<sub>3</sub><sup>-</sup> partitioning ratios  
348 are relatively stable, suggesting its general insensitivity in the predicted pH ranges (Nenes et al., 2020a).  
349 Changes in the SO<sub>4</sub><sup>2-</sup>, TNO<sub>3</sub> and NH<sub>x</sub> will result in  $\Delta$ pH of +0.18, -0.05 and -0.02 ~~units~~ from 2015 to

350 2050, respectively (Figure 6h).

351 With the strict control policy (SSP1-26-BHE), the emissions of SO<sub>2</sub>, NO<sub>x</sub> and NH<sub>3</sub> in 2050 will  
352 decrease by 86.9%, 74.9% and 41.7%, respectively, and the concentrations of SO<sub>4</sub><sup>2-</sup>, TNO<sub>3</sub> and NH<sub>x</sub>  
353 decrease substantially. The pH value will increase continuously by ~0.19 (from 3.36 in 2015 to 3.55 in  
354 2050). Changes in SO<sub>4</sub><sup>2-</sup> are more important determinants of ΔpH, resulting in ΔpH of +0.28-units from  
355 2015 to 2050. Changes in the TNO<sub>3</sub> and NH<sub>x</sub> are associated with 0.04 and 0.09 decreases in ΔpH,  
356 respectively. Moreover, the NO<sub>3</sub><sup>-</sup> and NH<sub>4</sub><sup>+</sup> partitioning ratios will decrease by 0.04 and 0.12, respectively,  
357 indicating a benefit of NH<sub>3</sub> and NO<sub>x</sub> emission controls in mitigating haze pollution in eastern China.

358 We also note that above analysis based on the historical average Δ<sub>aerosol</sub> / Δ<sub>(precursor emissions)</sub>  
359 ~~are-is~~ subject to uncertainties associated with changes in the atmospheric oxidation capacity,  
360 meteorological conditions, etc.. It is only a first-order estimation, and a full examination with 3-D  
361 chemical transport models ~~are-is~~ recommended in the future.



362

363 **Figure 6. Emissions of SO<sub>2</sub> (a), NO<sub>x</sub> (b), NH<sub>3</sub> (c), predicted pH (d), NO<sub>3</sub><sup>-</sup> partitioning (NO<sub>3</sub><sup>-</sup> / (NO<sub>3</sub><sup>-</sup> + HNO<sub>3</sub>))**  
364 **(e) and NH<sub>4</sub><sup>+</sup> partitioning (NH<sub>4</sub><sup>+</sup> / (NH<sub>4</sub><sup>+</sup> + NH<sub>3</sub>)) (f) in China from 2015 to 2050 under the three scenarios**  
365 **published in Tong et al.(Tong et al., 2020). Predicted contributions of individual factors to the ΔpH under the**

366 three scenarios, including SSP3-70-BAU (g), SSP2-45-ECP (h) and SSP1-26-BHE (i). The stacked color bars  
367 below the dashed line represent the factors that had negative impacts on  $\Delta\text{pH}$  and the stacked color bars  
368 above the dashed line represent the increase in  $\Delta\text{pH}$ . The meanings of the abbreviations:  $\text{NH}_x$ , total ammonia;  
369  $\text{TNO}_3$ , total nitrate; Oths, others.

#### 370 4 Conclusion

371 The aerosol pH values at an urban site in Shanghai during 2011–2019, for the first time, were modelled  
372 and reported using ISORROPIA II based on observed gas and aerosol composition. Although significant  
373 variations of aerosol compositions were observed from 2011 to 2019 in the YRD region, the aerosol pH  
374 estimated by model only slightly declined by 0.24 ~~unit~~. We quantified the contributions from individual  
375 factors to the variation of aerosol pH from 2011 to 2019. We found that besides the multiphase buffer  
376 effect,  $\text{SO}_4^{2-}$  and NVCs changes are key in regulating the aerosol pH from 2011 to 2019 in Shanghai.  
377  $\text{SO}_4^{2-}$  and NVCs showed an overall opposite effect on aerosol pH, with a contribution of +0.38 and  $-0.35$   
378 ~~unit~~, respectively.

379 Distinct seasonal variations in the aerosol pH were observed, with maximum and minimum aerosol  
380 pH of  $3.59 \pm 0.57$  in winter and  $2.89 \pm 0.49$  in summer, respectively. Seasonal variations in aerosol pH  
381 were mainly driven by the temperature, with the maximum  $\Delta\text{pH}$  of 0.63 between fall and winter. The  
382 diurnal cycle of aerosol pH was driven by the combined effects of temperature and RH which could result  
383 in  $\Delta\text{pH}$  of  $-0.22$  and  $+0.10$  ~~units~~, respectively. These results emphasized the importance of meteorological  
384 conditions in controlling the seasonal and diurnal variations of aerosol pH.

385 Finally, to explore the effects of China's future anthropogenic emission control pathways on aerosol  
386 pH and compositions, we chose three different emission reduction scenarios proposed by ~~Tong et al.~~ Tong  
387 et al. (2020) for future haze mitigation, naming SSP3-70-BAU, SSP2-45-ECP and SSP1-26-BHE as case  
388 studies. We found that under the weak control policy (SSP3-70-BAU), the future aerosol pH and  $\text{NO}_3^-$   
389 partitioning ratio will only have subtle changes. While our results also demonstrate that future aerosol  
390 pH will increase under both strict control policy (SSP1-26-BHE) and moderate control policy (SSP2-45-  
391 ECP) the former will result in a more dramatic increase. The significant increase in aerosol pH is mainly  
392 associated with the decrease in  $\text{SO}_4^{2-}$ . In addition, the increase in aerosol pH with strict control policy  
393 and moderate control policy will lead to relatively more nitrate and ammonium partitioning in the gas

394 phase, which is beneficial for future PM<sub>2.5</sub> pollution control. These results highlight the potential effects  
395 of precursors reductions on aerosol pH employing future pollution control policy.

#### 396 **Author Contributions**

397 HS, HW, and CH conceived and led the study. MZ conducted the field measurements and carried out the  
398 data analysis. MZ and GZ performed model simulations. MZ, HS, HW, CH, GZ, LQ, SZ, DH, YC, JA  
399 discussed the results. LQ, SZ, DH, SL, ST, QW, RY, YM, CC conducted the measurements at the station.  
400 MZ, HS and GZ wrote the manuscript with input from all co-authors.

#### 401 **Supplement**

402 The supplement is available in a separate file.

#### 403 **Competing interests**

404 The authors declare that they have no conflict of interest.

#### 405 **Data availability**

406 The data presented in this paper are available upon request from Hang Su ([h.su@mpic.de](mailto:h.su@mpic.de)) and Cheng  
407 Huang ([huangc@saes.sh.cn](mailto:huangc@saes.sh.cn)).

#### 408 **Acknowledgement**

409 This study was supported by the Science and Technology Commission of Shanghai Municipality Fund  
410 Project (20dz1204000), the National Key Research and Development Program of China  
411 (2018YFC0213800), , the General Fund of National Natural Science Foundation of China (21806108),  
412 the National Natural Science Foundation of China (42061134008), the Shanghai Rising-Star Program  
413 (19QB1402900) and Shanghai Municipal Bureau of Ecology and Environment Fund Project (2020-03).

#### 414 **Reference**

- 415 Battaglia Jr, M. A., Weber, R. J., Nenes, A., and Hennigan, C. J.: Effects of water-soluble organic carbon on aerosol  
416 pH, *Atmospheric Chemistry and Physics*, 19, 14607-14620, 10.5194/acp-19-14607-2019, 2019.
- 417 Battaglia, M. A., Douglas, S., and Hennigan, C. J.: Effect of the Urban Heat Island on Aerosol pH, *Environmental*  
418 *Science & Technology*, 51, 13095-13103, 10.1021/acs.est.7b02786, 2017.
- 419 Cai, S., Wang, Y., Zhao, B., Wang, S., Chang, X., and Hao, J.: The impact of the "Air Pollution Prevention and

420 Control Action Plan" on PM2.5 concentrations in Jing-Jin-Ji region during 2012-2020, *Sci Total Environ*, 580,  
421 197-209, 10.1016/j.scitotenv.2016.11.188, 2017.

422 Cheng, J., Su, J., Cui, T., Li, X., Dong, X., Sun, F., Yang, Y., Tong, D., Zheng, Y., Li, Y., Li, J., Zhang, Q., and He,  
423 K.: Dominant role of emission reduction in PM2.5 air quality improvement in Beijing during 2013–2017:  
424 a model-based decomposition analysis, *Atmospheric Chemistry and Physics*, 19, 6125-6146, 10.5194/acp-19-  
425 6125-2019, 2019.

426 Cheng, Y., Zheng, G., Wei, C., Mu, Q., Zheng, B., Wang, Z., Gao, M., Zhang, Q., He, K., Carmichael, G., Poscjl, U.,  
427 and Su, H.: Reactive nitrogen chemistry in aerosol water as a source of sulfate during haze events in China,  
428 *Science Advance*, 2016.

429 Clegg, S. L., Brimblecombe, P., and Wexler, A. S.: Thermodynamic Model of the System  $H^+-NH_4^+-Na^+-SO_4^{2-}$ -  
430  $-NO_3^- -Cl^- -H_2O$  at 298.15 K, *The Journal of Physical Chemistry A*, 102, 2155-2171, 10.1021/jp973043j,  
431 1998.

432 Ding, J., Zhao, P., Su, J., Dong, Q., Du, X., and Zhang, Y.: Aerosol pH and its driving factors in Beijing, *Atmospheric*  
433 *Chemistry and Physics*, 19, 7939-7954, 10.5194/acp-19-7939-2019, 2019.

434 Fang, T., Guo, H., Zeng, L., Verma, V., Nenes, A., and Weber, R. J.: Highly Acidic Ambient Particles, Soluble Metals,  
435 and Oxidative Potential: A Link between Sulfate and Aerosol Toxicity, *Environ Sci Technol*, 51, 2611-2620,  
436 10.1021/acs.est.6b06151, 2017.

437 Fountoukis, C. and Nenes, A.: ISORROPIA II: a computationally efficient thermodynamic equilibrium model for  
438  $K^+-Ca^{2+}-Mg^{2+}-NH_4^+-Na^+-SO_4^{2-}-NO_3^- -Cl^- -H_2O$  aerosols, *Atmospheric Chemistry and Physics*, 7,  
439 4639-4659, 2007.

440 Fu, X., Guo, H., Wang, X., Ding, X., He, Q., Liu, T., and Zhang, Z.: PM2.5 acidity at a background site in the Pearl  
441 River Delta region in fall-winter of 2007-2012, *J Hazard Mater*, 286, 484-492, 10.1016/j.jhazmat.2015.01.022,  
442 2015.

443 Guo, H., Weber, R. J., and Nenes, A.: High levels of ammonia do not raise fine particle pH sufficiently to yield  
444 nitrogen oxide-dominated sulfate production, *Sci Rep*, 7, 12109, 10.1038/s41598-017-11704-0, 2017a.

445 Guo, H., Otjes, R., Schlag, P., Kiendler-Scharr, A., Nenes, A., and Weber, R. J.: Effectiveness of ammonia reduction  
446 on control of fine particle nitrate, *Atmospheric Chemistry and Physics*, 18, 12241-12256, 10.5194/acp-18-  
447 12241-2018, 2018.

448 Guo, H., Liu, J., Froyd, K. D., Roberts, J. M., Veres, P. R., Hayes, P. L., Jimenez, J. L., Nenes, A., and Weber, R. J.:  
449 Fine particle pH and gas-particle phase partitioning of inorganic species in Pasadena, California, during the  
450 2010 CalNex campaign, *Atmospheric Chemistry and Physics*, 17, 5703-5719, 10.5194/acp-17-5703-2017,  
451 2017b.

452 Guo, H., Sullivan, A. P., Campuzano-Jost, P., Schroder, J. C., Lopez-Hilfiker, F. D., Dibb, J. E., Jimenez, J. L.,  
453 Thornton, J. A., Brown, S. S., Nenes, A., and Weber, R. J.: Fine particle pH and the partitioning of nitric acid  
454 during winter in the northeastern United States, *Journal of Geophysical Research: Atmospheres*, 121, 10,355-  
455 310,376, 10.1002/2016jd025311, 2016.

456 Guo, H., Xu, L., Bougiatioti, A., Cerully, K. M., Capps, S. L., Hite, J. R., Carlton, A. G., Lee, S. H., Bergin, M. H.,  
457 Ng, N. L., Nenes, A., and Weber, R. J.: Fine-particle water and pH in the southeastern United States,  
458 *Atmospheric Chemistry and Physics*, 15, 5211-5228, 10.5194/acp-15-5211-2015, 2015.

459 He, P., Alexander, B., Geng, L., Chi, X., Fan, S., Zhan, H., Kang, H., Zheng, G., Cheng, Y., Su, H., Liu, C., and Xie,  
460 Z.: Isotopic constraints on heterogeneous sulfate production in Beijing haze, *Atmospheric Chemistry and*  
461 *Physics*, 18, 5515-5528, 10.5194/acp-18-5515-2018, 2018.

462 Hennigan, C. J., Izumi, J., Sullivan, A. P., Weber, R. J., and Nenes, A.: A critical evaluation of proxy methods used  
463 to estimate the acidity of atmospheric particles, *Atmospheric Chemistry and Physics*, 15, 2775-2790,

464 10.5194/acp-15-2775-2015, 2015.

465 Huang, X. H. H., Bian, Q., Ng, W. M., Louie, P. K. K., and Yu, J. Z.: Characterization of PM<sub>2.5</sub> Major Components  
466 and Source Investigation in Suburban Hong Kong: A One Year Monitoring Study, *Aerosol and Air Quality*  
467 *Research*, 14, 237-250, 10.4209/aaqr.2013.01.0020, 2014.

468 Jia, S., Wang, X., Zhang, Q., Sarkar, S., Wu, L., Huang, M., Zhang, J., and Yang, L.: Technical note: Comparison  
469 and interconversion of pH based on different standard states for aerosol acidity characterization, *Atmospheric*  
470 *Chemistry and Physics*, 18, 11125-11133, 10.5194/acp-18-11125-2018, 2018.

471 Li, C., Hu, Y., Chen, J., Ma, Z., Ye, X., Yang, X., Wang, L., Wang, X., and Mellouki, A.: Physiochemical properties  
472 of carbonaceous aerosol from agricultural residue burning: Density, volatility, and hygroscopicity,  
473 *Atmospheric Environment*, 140, 94-105, 10.1016/j.atmosenv.2016.05.052, 2016.

474 Li, H., Cheng, J., Zhang, Q., Zheng, B., Zhang, Y., Zheng, G., and He, K.: Rapid transition in winter aerosol  
475 composition in Beijing from 2014 to 2017: response to clean air actions, *Atmospheric Chemistry and Physics*,  
476 19, 11485-11499, 10.5194/acp-19-11485-2019, 2019.

477 Li, W., Xu, L., Liu, X., Zhang, J., Lin, Y., Yao, X., Gao, H., Zhang, D., Chen, J., Wang, W., Harrison, R. M., Zhang,  
478 X., Shao, L., Fu, P., Nenes, A., and Shi, Z.: Air pollution–aerosol interactions produce more bioavailable iron  
479 for ocean ecosystems, *Science Advance*, 3, e1601749, 2017.

480 Liu, M., Huang, X., Song, Y., Xu, T., Wang, S., Wu, Z., Hu, M., Zhang, L., Zhang, Q., Pan, Y., Liu, X., and Zhu, T.:  
481 Rapid SO<sub>2</sub> emission reductions significantly increase tropospheric ammonia concentrations over the North  
482 China Plain, *Atmospheric Chemistry and Physics*, 18, 17933-17943, 10.5194/acp-18-17933-2018, 2018.

483 Masiol, M., Squizzato, S., Formenton, G., Khan, M. B., Hopke, P. K., Nenes, A., Pandis, S. N., Tositti, L., Benetello,  
484 F., Visin, F., and Pavoni, B.: Hybrid multiple-site mass closure and source apportionment of PM<sub>2.5</sub> and aerosol  
485 acidity at major cities in the Po Valley, *Sci Total Environ*, 704, 135287, 10.1016/j.scitotenv.2019.135287, 2020.

486 Nah, T., Guo, H., Sullivan, A. P., Chen, Y., Tanner, D. J., Nenes, A., Russell, A., Ng, N. L., Huey, L. G., and Weber,  
487 R. J.: Characterization of aerosol composition, aerosol acidity, and organic acid partitioning at an agriculturally  
488 intensive rural southeastern US site, *Atmospheric Chemistry and Physics*, 18, 11471-11491, 10.5194/acp-18-  
489 11471-2018, 2018.

490 Nenes, A., Pandis, S. N., Weber, R. J., and Russell, A.: Aerosol pH and liquid water content determine when  
491 particulate matter is sensitive to ammonia and nitrate availability, *Atmospheric Chemistry and Physics*, 20,  
492 3249-3258, 10.5194/acp-20-3249-2020, 2020a.

493 Nenes, A., Pandis, S. N., Kanakidou, M., Russell, A., Song, S., Vasilakos, P., and Weber, R. J.: Aerosol acidity and  
494 liquid water content regulate the dry deposition of inorganic reactive nitrogen, *Atmospheric Chemistry and*  
495 *Physics Discussion*, 10.5194/acp-2020-266, 2020b.

496 Nenes, A., Pandis, S. N., Kanakidou, M., Russell, A. G., Song, S., Vasilakos, P., and Weber, R. J.: Aerosol acidity  
497 and liquid water content regulate the dry deposition of inorganic reactive nitrogen, *Atmospheric Chemistry*  
498 *and Physics*, 21, 6023-6033, 10.5194/acp-21-6023-2021, 2021.

499 Pye, H. O. T., Zuend, A., Fry, J. L., Isaacman-VanWertz, G., Capps, S. L., Appel, K. W., Foroutan, H., Xu, L., Ng,  
500 N. L., and Goldstein, A. H.: Coupling of organic and inorganic aerosol systems and the effect on gas-particle  
501 partitioning in the southeastern US, *Atmos Chem Phys*, 18, 357-370, 10.5194/acp-18-357-2018, 2018.

502 Pye, H. O. T., Nenes, A., Alexander, B., Ault, A. P., Barth, M. C., Clegg, S. L., Collett Jr, J. L., Fahey, K. M.,  
503 Hennigan, C. J., Herrmann, H., Kanakidou, M., Kelly, J. T., Ku, I. T., McNeill, V. F., Riemer, N., Schaefer, T.,  
504 Shi, G., Tilgner, A., Walker, J. T., Wang, T., Weber, R., Xing, J., Zaveri, R. A., and Zuend, A.: The acidity of  
505 atmospheric particles and clouds, *Atmospheric Chemistry and Physics*, 20, 4809-4888, 10.5194/acp-20-4809-  
506 2020, 2020.

507 Qiao, L., Cai, J., Wang, H., Wang, W., Zhou, M., Lou, S., Chen, R., Dai, H., Chen, C., and Kan, H.: PM<sub>2.5</sub>

508 constituents and hospital emergency-room visits in Shanghai, China, *Environ Sci Technol*, 48, 10406-10414,  
509 10.1021/es501305k, 2014.

510 Rumsey, I. C., Cowen, K. A., Walker, J. T., Kelly, T. J., Hanft, E. A., Mishoe, K., Rogers, C., Proost, R., Beachley,  
511 G. M., Lear, G., Frelink, T., and Otjes, R. P.: An assessment of the performance of the Monitor for AeRosols  
512 and GAses in ambient air (MARGA): a semi-continuous method for soluble compounds, *Atmospheric*  
513 *Chemistry and Physics*, 14, 5639-5658, 10.5194/acp-14-5639-2014, 2014.

514 Shi, X., Zheng, Y., Lei, Y., Xue, W., Yan, G., Liu, X., Cai, B., Tong, D., and Wang, J.: Air quality benefits of achieving  
515 carbon neutrality in China, *Sci Total Environ*, 795, 148784, 10.1016/j.scitotenv.2021.148784, 2021.

516 Shi, X., Nenes, A., Xiao, Z., Song, S., Yu, H., Shi, G., Zhao, Q., Chen, K., Feng, Y., and Russell, A. G.: High-  
517 Resolution Data Sets Unravel the Effects of Sources and Meteorological Conditions on Nitrate and Its Gas-  
518 Particle Partitioning, *Environ Sci Technol*, 53, 3048-3057, 10.1021/acs.est.8b06524, 2019.

519 Song, S., Gao, M., Xu, W., Shao, J., Shi, G., Wang, S., Wang, Y., Sun, Y., and McElroy, M. B.: Fine-particle pH for  
520 Beijing winter haze as inferred from different thermodynamic equilibrium models, *Atmospheric Chemistry*  
521 *and Physics*, 18, 7423-7438, 10.5194/acp-18-7423-2018, 2018.

522 Stieger, B., Spindler, G., Fahlbusch, B., Müller, K., Grüner, A., Poulain, L., Thöni, L., Seidler, E., Wallasch, M., and  
523 Herrmann, H.: Measurements of PM10 ions and trace gases with the online system MARGA at the research  
524 station Melpitz in Germany – A five-year study, *Journal of Atmospheric Chemistry*, 75, 33-70,  
525 10.1007/s10874-017-9361-0, 2018.

526 Su, H., Cheng, Y., and Pöschl, U.: New Multiphase Chemical Processes Influencing Atmospheric Aerosols, Air  
527 Quality, and Climate in the Anthropocene, *Acc Chem Res*, 53, 2034-2043, 10.1021/acs.accounts.0c00246,  
528 2020.

529 Tan, T., Hu, M., Li, M., Guo, Q., Wu, Y., Fang, X., Gu, F., Wang, Y., and Wu, Z.: New insight into PM2.5 pollution  
530 patterns in Beijing based on one-year measurement of chemical compositions, *Sci Total Environ*, 621, 734-  
531 743, 10.1016/j.scitotenv.2017.11.208, 2018.

532 Tao, W., Su, H., Zheng, G., Wang, J., Wei, C., Liu, L., Ma, N., Li, M., Zhang, Q., Pöschl, U., and Cheng, Y.: Aerosol  
533 pH and chemical regimes of sulfate formation in aerosol water during winter haze in the North China Plain,  
534 *Atmospheric Chemistry and Physics*, 20, 11729-11746, 10.5194/acp-20-11729-2020, 2020.

535 Tao, Y. and Murphy, J. G.: The sensitivity of PM2.5 acidity to meteorological parameters and chemical composition  
536 changes: 10-year records from six Canadian monitoring sites, *Atmos. Chem. Phys.*, 19, 9309-9320,  
537 10.5194/acp-19-9309-2019, 2019.

538 Tilgner, A., Schaefer, T., Alexander, B., Barth, M., Collett Jr, J. L., Fahey, K. M., Nenes, A., Pye, H. O. T., Herrmann,  
539 H., and McNeill, V. F.: Acidity and the multiphase chemistry of atmospheric aqueous particles and clouds,  
540 *Atmospheric Chemistry and Physics*, 21, 13483-13536, 10.5194/acp-21-13483-2021, 2021.

541 Tong, D., Cheng, J., Liu, Y., Yu, S., Yan, L., Hong, C., Qin, Y., Zhao, H., Zheng, Y., Geng, G., Li, M., Liu, F., Zhang,  
542 Y., Zheng, B., Leon, C., and Zhang, Q.: Dynamic projection of anthropogenic emissions in China:  
543 methodology and 2015–2050 emission pathways under a range of socio-economic, climate policy, and  
544 pollution control scenarios, *Atmospheric Chemistry and Physics*, 20, 5729-5757, 10.5194/acp-20-5729-2020,  
545 2020.

546 Turpin, B. J. and Lim, H.-J.: Species Contributions to PM2.5 Mass Concentrations: Revisiting Common  
547 Assumptions for Estimating Organic Mass, *Aerosol Science and Technology*, 35, 602-610,  
548 10.1080/02786820119445, 2001.

549 Vasilakos, P., Russell, A., Weber, R., and Nenes, A.: Understanding nitrate formation in a world with less sulfate,  
550 *Atmospheric Chemistry and Physics*, 18, 12765-12775, 10.5194/acp-18-12765-2018, 2018.

551 Wang, H., Ding, J., Xu, J., Wen, J., Han, J., Wang, K., Shi, G., Feng, Y., Ivey, C. E., Wang, Y., Nenes, A., Zhao, Q.,

552 and Russell, A. G.: Aerosols in an arid environment: The role of aerosol water content, particulate acidity,  
553 precursors, and relative humidity on secondary inorganic aerosols, *Sci Total Environ*, 646, 564-572,  
554 10.1016/j.scitotenv.2018.07.321, 2019.

555 Wang, S., Wang, L., Li, Y., Wang, C., Wang, W., Yin, S., and Zhang, R.: Effect of ammonia on fine-particle pH in  
556 agricultural regions of China: comparison between urban and rural sites, *Atmospheric Chemistry and Physics*,  
557 20, 2719-2734, 10.5194/acp-20-2719-2020, 2020.

558 Weber, R. J., Guo, H., Russell, A. G., and Nenes, A.: High aerosol acidity despite declining atmospheric sulfate  
559 concentrations over the past 15 years, *Nature Geoscience*, 9, 282-285, 10.1038/ngeo2665, 2016.

560 Xie, Y., Wang, G., Wang, X., Chen, J., Chen, Y., Tang, G., Wang, L., Ge, S., Xue, G., Wang, Y., and Gao, J.: Nitrate-  
561 dominated PM<sub>2.5</sub> and elevation of particle pH observed in urban Beijing during the winter of 2017,  
562 *Atmospheric Chemistry and Physics*, 20, 5019-5033, 10.5194/acp-20-5019-2020, 2020.

563 Zheng, B., Tong, D., Li, M., Liu, F., Hong, C., Geng, G., Li, H., Li, X., Peng, L., Qi, J., Yan, L., Zhang, Y., Zhao, H.,  
564 Zheng, Y., He, K., and Zhang, Q.: Trends in China's anthropogenic emissions since 2010 as the consequence  
565 of clean air actions, *Atmospheric Chemistry and Physics*, 18, 14095-14111, 10.5194/acp-18-14095-2018, 2018.

566 Zheng, G., Su, H., Wang, S., Andreae, M. O., Poschl, U., and Cheng, Y.: Multiphase buffer theory explains contrasts  
567 in atmospheric aerosol acidity, *Science* 369, 1374-1377, 2020.

568 Zhou, M., Qiao, L., Zhu, S., Li, L., Lou, S., Wang, H., Wang, Q., Tao, S., Huang, C., and Chen, C.: Chemical  
569 characteristics of fine particles and their impact on visibility impairment in Shanghai based on a 1-year period  
570 observation, *J Environ Sci (China)*, 48, 151-160, 10.1016/j.jes.2016.01.022, 2016.

571